Observation of Non-Hermitian Edge Burst Effect in One-Dimensional Photonic Quantum Walk

Jiankun Zhu,[1,*] Ya-Li Mao,[1,*] Hu Chen,[1] Kui-Xing Yang,[1] Linhu Li,[2,†] Bing Yang,[1,‡] Zheng-Da Li,[1,§] and Jingyun Fan[1,3,‖]

[1]*Department of Physics and Shenzhen Institute for Quantum Science and Engineering, Southern University of Science and Technology, Shenzhen, 518055, China*

[2]*Guangdong Provincial Key Laboratory of Quantum Metrology and Sensing and School of Physics and Astronomy, Sun Yat-Sen University (Zhuhai Campus), Zhuhai 519082, China*

[3]*Center for Advanced Light Source, Southern University of Science and Technology, Shenzhen 518055, China*

(Received 22 October 2023; accepted 19 April 2024; published 17 May 2024)

Non-Hermitian systems can exhibit unique quantum phases without any Hermitian counterparts. For example, the latest theoretical studies predict a new surprising phenomenon that bulk bands can localize and dissipate prominently at the system boundary, which is dubbed the non-Hermitian edge burst effect. Here we realize a one-dimensional non-Hermitian Su-Schrieffer-Heeger lattice with bulk translation symmetry implemented with a photonic quantum walk. Employing time-resolved single-photon detection to characterize the chiral motion and boundary localization of bulk bands, we determine experimentally that the dynamics underlying the non-Hermitian edge burst effect is due to the interplay of non-Hermitian skin effect and imaginary band gap closing. This new non-Hermitian physical effect deepens our understanding of quantum dynamics in open quantum systems.

DOI: 10.1103/PhysRevLett.132.203801

Introduction.—Non-Hermitian physics provides an efficient and intuitive description of open quantum systems with dissipation, revealing many intriguing phenomena beyond the Hermitian scenario [1–49]. The seminal non-Hermitian skin effect (NHSE) showcases the bulk band localization towards the boundary [8–12], which generalizes the bulk-boundary correspondence as a fundamental principle of topological quantum phases [8,15,17]. NHSE has been a focused topic of contemporary research both experimentally and theoretically [8–12,14–19,21–27,29,30,32–38,40–43,45], unveiling many exotic statistical and dynamical properties when interplaying with other mechanisms. Regarding dissipation as a defining property of open quantum systems, NHSE, in synergy with imaginary band gap closing, generates a surprising result by predicting the prominent dissipation of bulk band at the boundary, which is dubbed the non-Hermitian edge burst effect (NHEBE) [44]. While NHEBE was originally predicted in an open system with spatially homogeneous loss, it turns out that a system with spatially inhomogeneous loss can also host NHEBE [48], suggesting that NHEBE may widely exist.

Along with the rapid theoretical advance, here we report the experimental realization of NHEBE in a Su-Schrieffer-Heeger (SSH) lattice. The lattice is implemented with photonic quantum walk in the time domain [26,39,45–47,50–53], possessing spatially homogeneous dissipation. By employing the time-resolved single-photon detection to detect the dissipation of photon pulse from each unit cell, we observe the chiral motion and bulk-band localization towards the boundary *in situ* and determine experimentally the underlying mechanism responsible for the birth of NHEBE for the lattice under study.

The 1D non-Hermitian Floquet SSH model.—We consider a one-dimensional lattice of size N with each cell containing two sites A and B and denote the state at each site respectively as $|n,A\rangle$ and $|n,B\rangle$ with $n = 1, 2, \ldots, N$, as sketched in Fig. 1(a). We consider three types of elementary dynamical processes which are intracell hopping between $|n,A\rangle$ and $|n,B\rangle$ characterized by the operator U_1, intercell hopping between $|n,B\rangle$ and $|n+1,A\rangle$ described by the hopping operator U_2, and dissipation Γ on the superposition state $|n,-\rangle$ at a rate of $e^{-\gamma}$ with $|n,\pm\rangle = (|n,A\rangle \pm |n,B\rangle)/\sqrt{2}$. The intercell hopping operator comprises operator $R(t) = \left[\begin{smallmatrix}\sqrt{1-t} & \sqrt{t} \\ -\sqrt{t} & \sqrt{1-t}\end{smallmatrix}\right]$ and the stagger operator $S = \sum(|n-1,A\rangle\langle n,A| + |n,B\rangle\langle n,B|)$. Hence the transport behavior on the SSH lattice is governed by the Floquet operator,

$$\mathcal{F} = U_2 U_1 \Gamma \tag{1}$$

where

$$\begin{aligned}\Gamma &= I_{\mathrm{ex}} \otimes (|+\rangle\langle +| + e^{-\gamma}|-\rangle\langle -|),\\ U_1 &= I_{\mathrm{ex}} \otimes R(t_1),\\ U_2 &= S^{-1}\left[\sum_{n=1}^{N-1}|n\rangle\langle n| \otimes R(t_2) + |N\rangle\langle N| \otimes I_{\mathrm{in}}\right]S,\end{aligned} \tag{2}$$

 © 2024 American Physical Society

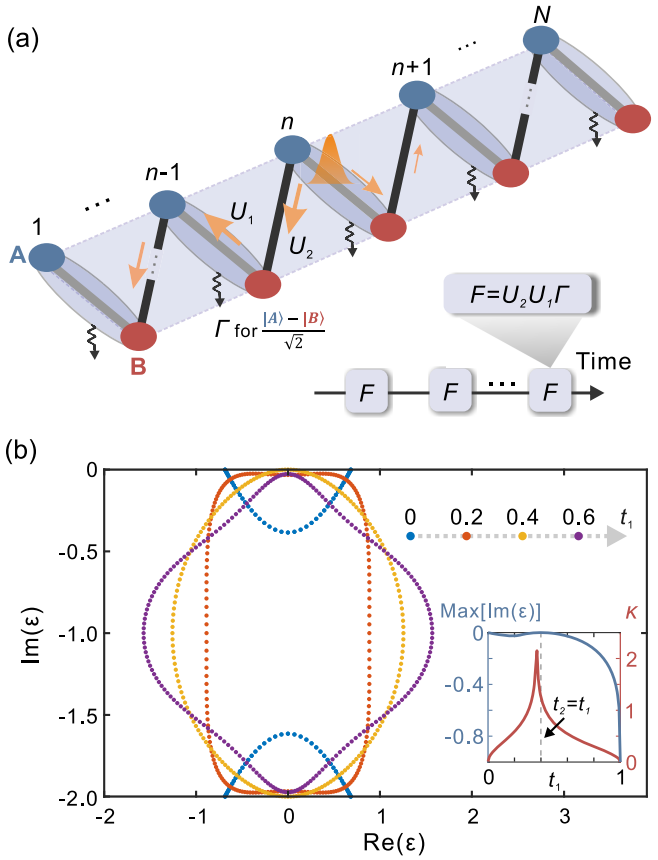

FIG. 1. The non-Hermitian SSH lattice model. (a) We draw the non-Hermitian SSH lattice model as two sublattices with the nearest neighbor coupling U_1 and U_2. The dissipation Γ occurs only via the superposition state $|n,-\rangle = (|n,A\rangle - |n,B\rangle)/\sqrt{2}$. Then we can describe the single particle transport in this lattice by the Floquet operator $F = U_2U_1\Gamma$. (b) The respective energy spectra with intercell hopping paramter $t_2 = 0.40$ and $\gamma = 2.00$. Inset: the maxima of the imaginary gaps and the NHSE parameter κ versus intercell hopping parameter t_1.

with I_{in} the identity operator acting on the internal degree-of-freedom (within the unit cell), $I_{\text{ex}} = \sum_{n=1}^{N} |n\rangle\langle n|$ the $N \times N$ identity operator of the external degree-of-freedom (between unit cells), and t_1 (t_2) the intra- (inter-) cell hopping parameter.

Since an initial state prepared inside the bulk is insensitive to boundary conditions before it evolves to the boundary of the system, one may gain intuition of NHEBE by examining the system under the periodic boundary condition (PBC). Replacing I_{in} in Eq. (2) with $R(t_2)$ and setting $|N,\cdot\rangle = |0,\cdot\rangle$ to satisfy PBC, we calculate the quasienergies ϵ of the effective Hamiltonian $H_{\text{PBC}} = i \ln \mathcal{F}_{\text{PBC}}$, where $\mathcal{F}_{PBC}$ is the respective Floquet operator. Some remarks are in order. (i) $\mathcal{F}_{PBC}$ has a conjugated particle-hole symmetry supporting nontrivial 1D topological properties [54]. (ii) For $\gamma \neq 0$, the PBC quasi-spectrum encloses a finite area in the complex quasienergy plane [see Fig. 1(b)], indicating the emergence of NHSE of the system under open boundary condition (OBC) [21,24,28]. The numerical study shows that NHSE is most significant at $t_1 \approx 0.13$ where the inverse localization length κ of OBC skin eigenstates maximizes [red smooth line in the inset of Fig. 1(b)]. (iii) The imaginary quasienergy gap $\text{Max}[\text{Im}(\epsilon)]$ [blue smooth line in the inset of Fig. 1(b)] remains small for $t_1 < t_2$ and closes at $t_1 = t_2$. The imaginary gap closing is associated with a topological phase transition of the Hermitian counterpart of our model (see Supplemental Material [54]). The imaginary gap closing of the PBC quasispectrum implies the lossless propagation of state toward the accumulating direction of NHSE. Accordingly, a state with a small dissipation rate in the bulk of a finite system may reach the boundary before it is completely dissipated during the evolution, resulting in NHEBE. Hence, the interplay of NHSE and imaginary gap closing shall lead to the emergence of NHEBE in the system under study [44].

Experimental realization of NHEBE.—The experimental schematic to realize the Floquet-SSH model employing quantum walk in the time domain is depicted in Fig. 2. We recycle a single-photon pulse (walker) in an optical loop, where the unit cell of the lattice is the time-bin (8 ns) containing the photon pulse and the lattice constant ($\tau_a = 44$ ns) is the time difference between photons traversing the long and short arms of the Mach-Zehnder interferometer (MZI). Site A (B) in the unit cell corresponds to the horizontal (vertical) polarization state $|H\rangle$ ($|V\rangle$). The walker completes one-step time evolution in the lattice as the photon pulse completes a cycle within $\tau_c (= 9550$ ns). We create a one-dimensional lattice of size $N(= 17)$ by packing N time bins with $N\tau_a < \tau_c$. We note that a single-photon wave function self-interferes when tunneling between adjacent lattice sites, manifesting the quantum effect.

Our experimental setup shares similarities with previous experiments [26,39,45–47,50–53], but there are distinct differences. As shown in Fig. 2(a) and illustrated in Fig. 2(b), we introduce dissipation to the superposition state $|n,-\rangle = (|n,A\rangle - |n,B\rangle)/\sqrt{2}$ by passing the photon pulse through a customized polarizing beam splitter (CPBS), which transmits photons in state $|+\rangle$ with unity probability and reflects photons in state $|-\rangle$ with a probability of $(1 - e^{-2\gamma})$. In order to realize the intercell hopping U_2, we implement the stagger operator S (S^{-1}) by letting photons in state $|H\rangle$ step forward (backward) by one time bin using the first (second) MZI and implement the rotation $R(t_2)$ by passing photons through an electro-optical-modulator (EOM) and an HWP between the two MZIs. We implement the intracell hopping U_1 by passing the photon pulse through a pair of half-wave plates (HWP). Different from previous experiments, we generate the OBC by controlling the time sequence of the EOM such that $R(t_2)$ only acts on $(N-1)$ cells of the lattice, hence defining the first and last unit cells of the lattice (see Supplemental Material [54]).

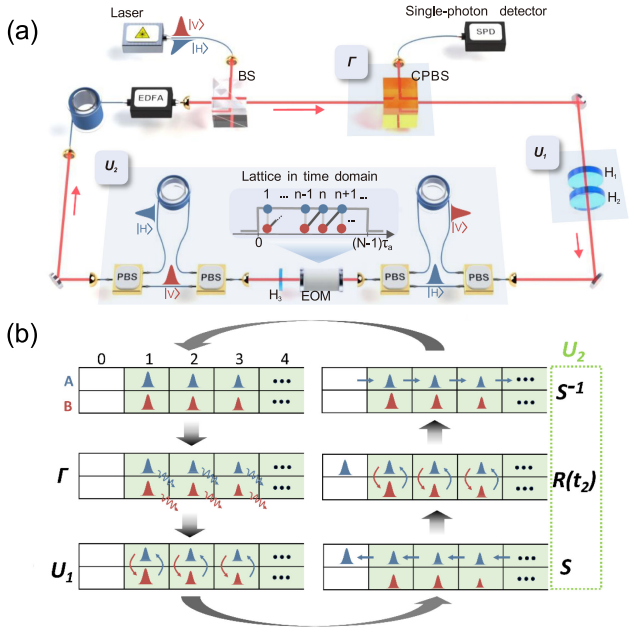

FIG. 2. Schematic of the experimental setup. (a) To implement the photonic quantum walk, we couple 10% energy of laser pulses ($\lambda = 1560$ nm) into an optical loop via a beam splitter (BS). We pass them through a customized polarizing beam splitter (CPBS) to induce dissipation Γ, a pair of half-wave plates (H_1 and H_2) to implement the intracell tunneling U_1, then through an unbalanced Mach-Zehnder interferometer (MZI), an electro-optical-modulator (EOM), and the second MZI to implement the intercell tunneling U_2 (see main text and Supplemental Material [54]). We apply time-resolved single-photon detection to the dissipation from the CPBS. We note that the time sequences for the laser diode, the EOM, and the single-photon detecter are precisely synchronized. Additionally, an erbium-doped fiber amplifier (EDFA) is integrated into the loop to mitigate the optical loss. (b) An illustration to realize the Floquet operator in Eq. (1), here creating an edge at the boundary of the lattices to implement the OBC.

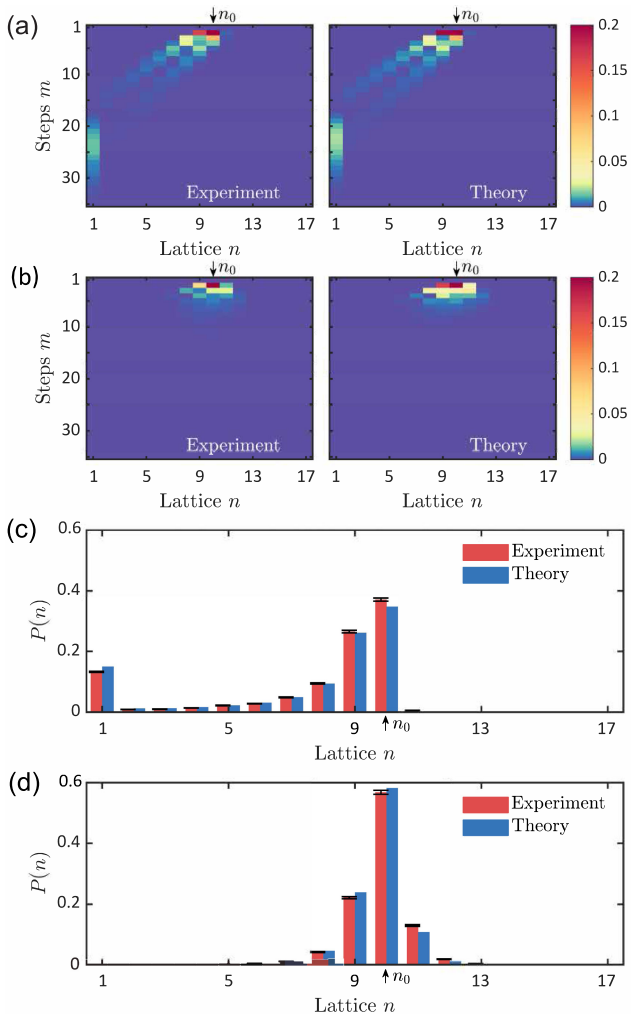

FIG. 3. Experimental measurements of photon dissipations. (a) and (b) Photon dissipation probabilities $p(n, m)$ with $|\phi_0\rangle = |10, +\rangle$, $N = 17$, $t_1 = t_2 = 0.4$ in (a), and $t_1 = 0.88$, $t_2 = 0.4$ in (b). Left (right) panel: experimental (theoretical) results with high (low) dissipation in red (blue). (c) and (d) Accumulated dissipations $P(n)$ that correspond, respectively, to (a) and (b), with experimental (thoretical) results drawn in red (blue). Error bars stand for 1 standard deviation.

By precisely coordinating the time of a laser diode to emit a photon pulse and the time to apply a 704 ns voltage pulse on EOM to execute the operation $R(t_2)$, we prepare the initial state $|\phi_0\rangle = |n_0, +\rangle$ by placing the photon pulse in the n_0^{th} unit cell. The accumulated 5.5 dB photon loss in the optical loop, which includes the loss due to the beam splitter (BS) to couple 10% energy of the photon pulse emitted by the laser diode into the optical loop, is mitigated using a polarization-independent erbium doped fiber amplifier (EDFA) [46,47]. Finally, by applying the time-resolved single-photon detection to the dissipation via the CPBS, we obtain the dissipation probability of the n_0^{th} cell after m steps of time evolution as $p(n, m) = N_{\text{photon}}(n, m)/\sum_{n'=1}^{N}\sum_{m'=1}^{M} N_{\text{photon}}(n', m')$, where $N_{\text{photon}}(n, m)$ is the respective number of detected photons, and the accumulated dissipation per site as $P(n) = \sum_{m=1}^{M} p(n, m)$.

We present in Fig. 3 the dissipation measured in two experimental scenarios, where we set commonly the initial state of single photons to $|\phi_0\rangle = |10, +\rangle$, $\gamma = 2.00$, $N = 17$ and 35 time steps, and set $t_1 = t_2 = 0.40$ in one experiment [left panel, Fig. 3(a)] and $t_1 = 0.88$, $t_2 = 0.40$ in the second [left panel, Fig. 3(b)]. (We use this set of parameters throughout unless otherwise specified in this Letter.) We notice that the measured dissipation probabilities in both experiments indicate that single photons *walk* towards the left boundary of the lattice. This net chiral motion is attributed to NHSE with all bulk bands of eigenstates localized towards the left boundary. The accumulated dissipation $P(n)$ continues to decrease as the single photon walks further away from the initial lattice site and towards the left boundary in both experiments [Figs. 3(c) and 3(d)]. While $P(n)$ is most significant at sites around n_0 and quickly becomes negligible with $P_{\text{edge}}^{c} = P(1) = 0.03\%$ in

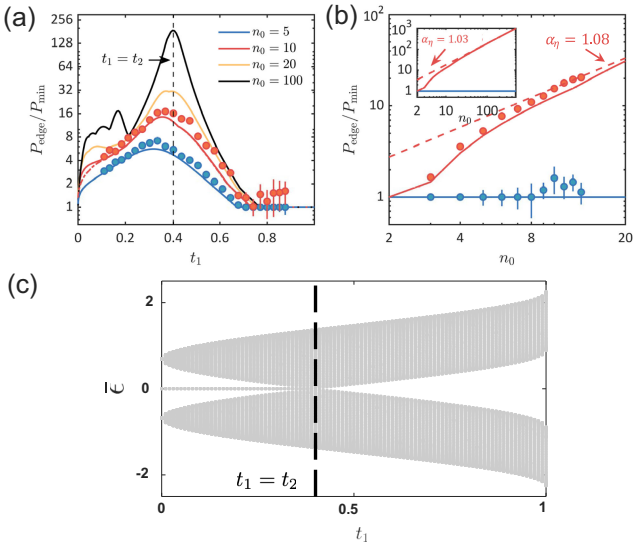

FIG. 4. Characteristic features of the non-Hermitian edge burst effect. (a) $P_{\text{edge}}/P_{\text{min}}$ versus intercell hopping parameter t_1. Smooth lines from top to bottom are numerical results with $(n_0, N) = (100, 200), (20, 40), (10, 17), (5, 17),$ respectively. Filled dots: the respective experimental results. (b) The scaling relation. Red smooth lines (numerical) and red solid dots (experimental) are for $t_1 = t_2$. Red dashed line is the scaling relation with $\alpha_\mu = 1.08$. Inset: Red smooth line is the numerical result and red dashed line is the scaling relation with $\alpha_\mu = 1.03$ for $n \leq 500$. Respectively, blue lines (numerical) and blue solid dots (experimental) are for $t_1 > t_2$. Error bars stand for 1 standard deviation. (c) Quasienergy spectrum $\bar{\epsilon}$ under OBC for the system described by the unitary Floquet operator U_2U_1 with $t_2 = 0.4$. A pair of zero-energy edge states are seen in the parameter region of $0 < t_1 < t_2$, and a topological phase transition occurs at $t_1 = t_2$.

the second experiment [Fig. 3(d)], the decreasing trend of $P(n)$ in the first experiment [Fig. 3(c)] is upended with $P(n)$ at the boundary suddenly jumping to a significant value with $P^b_{\text{edge}} = P(1) = 13.3\%$. The large contrast of $P^b_{\text{edge}}/P^c_{\text{edge}} > 400$ signifies NHEBE in the first experiment [Fig. 3(c)]. We have faithfully reproduced the experimental observations numerically (see Fig. 3).

Denote $P_{\text{min}} = \min\{P(1), P(2), \ldots, P(n_0)\}$, we experimentally observe $P_{\text{edge}}/P_{\text{min}} \gg 1$ for a broad range of parameter values of t_1 (red solid dots) with the maximum at $t_1 = 0.38$ as shown in Fig. 4(a). We observe similar results for $n_0 = 5$ with the maximum at $t_1 = 0.35$ (blue solid dots), for which the imaginary gap opens [see the inset of Fig. 1(b)]. As shown in Fig. 4(b), the experimental results of $P_{\text{edge}}/P_{\text{min}}$ versus n_0 under the condition of $t_1 = t_2 = 0.4$ (red solid dots) indicate a power law relation for increasing n_0, $P_{\text{edge}}/P_{\text{min}} \propto n_0^{\alpha_\eta}$ with $\alpha_\eta = 1.08$, which is in reasonable agreement with $\alpha_\eta = 1$ of the analytical result and referred to as a bulk-edge scaling relation underlying NHEBE for the system under study [44]. In contrast, the experimental data under the condition of $t_1 = 0.88$ and $t_2 = 0.4$ (blue solid dots) shows that $P_{\text{edge}}/P_{\text{min}} \sim 1$, deviating from the power law relation, which is consistent with the expectation of the absence of NHEBE in this parameter regime. In these studies, the numerical results (smooth lines in Fig. 4) and experimental results consistently uphold a good agreement, verifying that the numerical analysis faithfully emulates our experiment. This inspires numerical experiments with much bigger system sizes. We plot the numerical results for $n_0 = 20$ (orange smooth line) and $n_0 = 100$ (black smooth line) in Fig. 4(a), which indicates that the peak position of $P_{\text{edge}}/P_{\text{min}}$ monotonically converges to $t_1 = t_2$ for increasing lattice size and NHEBE is more pronounced at $t_1 = t_2$ [44]. Numerical experiments with system size up to 500 lattice sites yield $\alpha_\eta = 1.03$ as shown in the inset of Fig. 4(b), indicating that the insignificant quantitative difference diminishes when the system is sufficiently large.

Discussion.—In our studies, we reveal that P_{edge} is negligible in the non-NHEBE regime and significant in the NHEBE regime. Compared to measuring the dissipation properties in the bulk of the system, detecting the dissipation effect at the physical boundary is more experimentally accessible. Intriguingly, dissipation has been recently used to study the bulk topological invariants of Bloch bands below a cutoff energy [55]. This is done by filtering out the unwanted higher-band components through dissipation. In comparison, we find that the NHEBE in our setting, which can be observed in a single measurement, provides a method to detect Hermitian topological phase transitions through a probe of the nonunitary dissipation. Explicitly, we rewrite the Floquet operator in the momentum space,

$$\mathcal{F}_{\text{PBC}}(k) = \left[h_0\sigma_0 + i\sum_{\alpha=x,y,z} h_\alpha(k)\sigma_\alpha\right]\Gamma_k = \bar{\mathcal{F}}_{\text{PBC}}(k)\gamma_k, \quad (3)$$

where the dissipation $\Gamma_k = |+\rangle\langle+| + e^{-\gamma}|-\rangle\langle-|$ takes the same form as in real space. For a general two-band non-Hermitian system described by the unitary Floquet operator $\bar{\mathcal{F}}_{\text{PBC}}(k)$, possible topological phase transitions require gap closing between the two bands, which is determined by $h_x = h_y = h_z = 0$. Consequently, $\bar{\mathcal{F}}_{\text{PBC}}(k)$ becomes an identity matrix and does not mix the two components of $|\pm\rangle$ with and without dissipation, respectively. Therefore, the dissipation-free component ($|+\rangle$ in our example) is governed by a unitary evolution at the topological phase transition point, corresponding to the closing of imaginary gap and hence manifesting as the most prominent NHEBE. Indeed, as shown in Fig. 4(c), a topological phase transition for the unitary part of our Floquet operator (U_2U_1) occurs at $t_1 = t_2$, which manifests by the steep $P_{\text{edge}}/P_{\text{min}}$ around $t_1 = t_2$ in Fig. 4(a).

In summary, we have experimentally demonstrated the observation of NHEBE in a SSH lattice possessing bulk translation symmetry, where the birth of NHEBE is due to the interplay of NHSE and imaginary band gap closing [44].

We noted that a system breaking the bulk translation symmetry may also host NHEBE, where NHSE is absent [48]. Hence, NHEBE may widely occur in many-body systems and is linked to different physical properties depending on its specific realization, which needs further exploration at both theoretical and experimental sides. In the regime of NHEBE, the dissipation becomes significant at the boundary and accessible to detection, which may inspire novel utilities such as the detection of topological phase transitions of the counterpart Hermitian system as discussed in the above. Explicitly, a Hermitian topological phase transition usually accompanies vanishing Pauli matrices in its unitary Floquet operator, corresponding to the imaginary gap closing in the counterpart non-Hermitian system with nonunitary dissipation (see Supplemental Material [54]).

Note added.—After completing this work, we became aware of a related experiment conducted by L. Xiao *et al.* [56].

This work is supported by the Key-Area Research and Development Program of Guangdong Province Grant No. 2020B0303010001, Grant No. 2019ZT08X324, Guangdong Provincial Key Laboratory Grant No. 2019B121203002, the National Natural Science Foundation of China Grants No. 12005090, and the Shenzhen Science and Technology Program Grants No. RCYX20210706092043065, No. JCYJ20220530113404009. B. Y. acknowledges support from the National Key R&D Program of China (Grant No. 2022YFA1405800), NNSFC (Grant No. 12274199), Guangdong Major Project of Basic and Applied Basic Research (Grant No. 2023B0303000011) and the Stable Support Plan Program of Shenzhen Natural Science Fund (Grant No. 20220815092422002). L. L. acknowledges support from the National Natural Science Foundation of China (Grant No. 12104519) and the Guangdong Project (Grant No. 2021QN02X073).

[*]These authors contributed equally to this work.
[†]lilh56@mail.sysu.edu.cn
[‡]yangbing@sustech.edu.cn
[§]lizd@sustech.edu.cn
[‖]fanjy@sustech.edu.cn

[1] H. J. Carmichael, Quantum trajectory theory for cascaded open systems, Phys. Rev. Lett. **70**, 2273 (1993).
[2] C. M. Bender and S. Boettcher, Real spectra in non-Hermitian Hamiltonians having pt symmetry, Phys. Rev. Lett. **80**, 5243 (1998).
[3] C. M. Bender, Making sense of non-Hermitian Hamiltonians, Rep. Prog. Phys. **70**, 947 (2007).
[4] I. Rotter, A non-Hermitian Hamilton operator and the physics of open quantum systems, J. Phys. A **42**, 153001 (2009).
[5] J. M. Zeuner, M. C. Rechtsman, Y. Plotnik, Y. Lumer, S. Nolte, M. S. Rudner, M. Segev, and A. Szameit, Observation of a topological transition in the bulk of a non-Hermitian system, Phys. Rev. Lett. **115**, 040402 (2015).
[6] T. E. Lee, Anomalous edge state in a non-Hermitian lattice, Phys. Rev. Lett. **116**, 133903 (2016).
[7] X. Zhan, L. Xiao, Z. Bian, K. Wang, X. Qiu, B. C. Sanders, W. Yi, and P. Xue, Detecting topological invariants in nonunitary discrete-time quantum walks, Phys. Rev. Lett. **119**, 130501 (2017).
[8] S. Yao and Z. Wang, Edge states and topological invariants of non-Hermitian systems, Phys. Rev. Lett. **121**, 086803 (2018).
[9] S. Yao, F. Song, and Z. Wang, Non-Hermitian Chern bands, Phys. Rev. Lett. **121**, 136802 (2018).
[10] F. K. Kunst, E. Edvardsson, J. C. Budich, and E. J. Bergholtz, Biorthogonal bulk-boundary correspondence in non-Hermitian systems, Phys. Rev. Lett. **121**, 026808 (2018).
[11] V. M. Martinez Alvarez, J. E. Barrios Vargas, and L. E. F. Foa Torres, Non-Hermitian robust edge states in one dimension: Anomalous localization and eigenspace condensation at exceptional points, Phys. Rev. B **97**, 121401(R) (2018).
[12] Y. Xiong, Why does bulk boundary correspondence fail in some non-Hermitian topological models, J. Phys. Commun. **2**, 035043 (2018).
[13] A. McDonald, T. Pereg-Barnea, and A. A. Clerk, Phase-dependent chiral transport and effective non-Hermitian dynamics in a bosonic Kitaev-Majorana chain, Phys. Rev. X **8**, 041031 (2018).
[14] C. H. Lee, L. Li, and J. Gong, Hybrid higher-order skin-topological modes in nonreciprocal systems, Phys. Rev. Lett. **123**, 016805 (2019).
[15] K. Yokomizo and S. Murakami, Non-Bloch band theory of non-Hermitian systems, Phys. Rev. Lett. **123**, 066404 (2019).
[16] K. Kawabata, K. Shiozaki, M. Ueda, and M. Sato, Symmetry and topology in non-Hermitian physics, Phys. Rev. X **9**, 041015 (2019).
[17] C. H. Lee and R. Thomale, Anatomy of skin modes and topology in non-Hermitian systems, Phys. Rev. B **99**, 201103(R) (2019).
[18] S. Longhi, Topological phase transition in non-Hermitian quasicrystals, Phys. Rev. Lett. **122**, 237601 (2019).
[19] F. K. Kunst and V. Dwivedi, Non-Hermitian systems and topology: A transfer-matrix perspective, Phys. Rev. B **99**, 245116 (2019).
[20] Y. Ashida, Z. Gong, and M. Ueda, Non-Hermitian physics, Adv. Phys. **69**, 249 (2020).
[21] K. Zhang, Z. Yang, and C. Fang, Correspondence between winding numbers and skin modes in non-Hermitian systems, Phys. Rev. Lett. **125**, 126402 (2020).
[22] L. Li, C. H. Lee, S. Mu, and J. Gong, Critical non-Hermitian skin effect, Nat. Commun. **11**, 5491 (2020).
[23] L. Li, C. H. Lee, and J. Gong, Topological switch for non-Hermitian skin effect in cold-atom systems with loss, Phys. Rev. Lett. **124**, 250402 (2020).
[24] N. Okuma, K. Kawabata, K. Shiozaki, and M. Sato, Topological origin of non-Hermitian skin effects, Phys. Rev. Lett. **124**, 086801 (2020).
[25] T. Helbig, T. Hofmann, S. Imhof, M. Abdelghany, T. Kiessling, L. W. Molenkamp, C. H. Lee, A. Szameit, M. Greiter, and R. Thomale, Generalized bulk–boundary

correspondence in non-Hermitian topolectrical circuits, Nat. Phys. **16**, 747 (2020).
[26] S. Weidemann, M. Kremer, T. Helbig, T. Hofmann, A. Stegmaier, M. Greiter, R. Thomale, and A. Szameit, Topological funneling of light, Science **368**, 311 (2020).
[27] L. Xiao, T. Deng, K. Wang, G. Zhu, Z. Wang, W. Yi, and P. Xue, Non-Hermitian bulk-boundary correspondence in quantum dynamics, Nat. Phys. **16**, 761 (2020).
[28] D. S. Borgnia, A. J. Kruchkov, and R.-J. Slager, Non-Hermitian boundary modes and topology, Phys. Rev. Lett. **124**, 056802 (2020).
[29] A. Ghatak, M. Brandenbourger, J. Van Wezel, and C. Coulais, Observation of non-Hermitian topology and its bulk-edge correspondence in an active mechanical metamaterial, Proc. Natl. Acad. Sci. U.S.A. **117**, 29561 (2020).
[30] C.-X. Guo, C.-H. Liu, X.-M. Zhao, Y. Liu, and S. Chen, Exact solution of non-Hermitian systems with generalized boundary conditions: Size-dependent boundary effect and fragility of the skin effect, Phys. Rev. Lett. **127**, 116801 (2021).
[31] E. J. Bergholtz, J. C. Budich, and F. K. Kunst, Exceptional topology of non-Hermitian systems, Rev. Mod. Phys. **93**, 015005 (2021).
[32] S. Liu, R. Shao, S. Ma, L. Zhang, O. You, H. Wu, Y. J. Xiang, T. J. Cui, and S. Zhang, Non-Hermitian skin effect in a non-Hermitian electrical circuit, Research **2021**, 5608038 (2021).
[33] M. Lu, X.-X. Zhang, and M. Franz, Magnetic suppression of non-Hermitian skin effects, Phys. Rev. Lett. **127**, 256402 (2021).
[34] X.-Q. Sun, P. Zhu, and T. L. Hughes, Geometric response and disclination-induced skin effects in non-Hermitian systems, Phys. Rev. Lett. **127**, 066401 (2021).
[35] X. Zhang, Y. Tian, J.-H. Jiang, M.-H. Lu, and Y.-F. Chen, Observation of higher-order non-Hermitian skin effect, Nat. Commun. **12**, 5377 (2021).
[36] L. Zhang, Y. Yang, Y. Ge, Y.-J. Guan, Q. Chen, Q. Yan, F. Chen, R. Xi, Y. Li, D. Jia *et al.*, Acoustic non-Hermitian skin effect from twisted winding topology, Nat. Commun. **12**, 6297 (2021).
[37] L. S. Palacios, S. Tchoumakov, M. Guix, I. Pagonabarraga, S. Sánchez, and A. G Grushin, Guided accumulation of active particles by topological design of a second-order skin effect, Nat. Commun. **12**, 1 (2021).
[38] L. Xiao, T. Deng, K. Wang, Z. Wang, W. Yi, and P. Xue, Observation of non-Bloch parity-time symmetry and exceptional points, Phys. Rev. Lett. **126**, 230402 (2021).
[39] Q. Lin, T. Li, L. Xiao, K. Wang, W. Yi, and P. Xue, Observation of non-Hermitian topological anderson insulator in quantum dynamics, Nat. Commun. **13**, 3229 (2022).
[40] S. Longhi, Self-healing of non-Hermitian topological skin modes, Phys. Rev. Lett. **128**, 157601 (2022).
[41] Q. Liang, D. Xie, Z. Dong, H. Li, H. Li, B. Gadway, W. Yi, and B. Yan, Observation of non-Hermitian skin effect and topology in ultracold atoms, Phys. Rev. Lett. **129**, 070401 (2022).
[42] K. Zhang, Z. Yang, and C. Fang, Universal non-Hermitian skin effect in two and higher dimensions, Nat. Commun. **13**, 2496 (2022).
[43] Q. Liang, D. Xie, Z. Dong, H. Li, H. Li, B. Gadway, W. Yi, and B. Yan, Dynamic signatures of non-Hermitian skin effect and topology in ultracold atoms, Phys. Rev. Lett. **129**, 070401 (2022).
[44] W.-T. Xue, Y.-M. Hu, F. Song, and Z. Wang, Non-Hermitian edge burst, Phys. Rev. Lett. **128**, 120401 (2022).
[45] Q. Lin, T. Li, L. Xiao, K. Wang, W. Yi, and P. Xue, Topological phase transitions and mobility edges in non-Hermitian quasicrystals, Phys. Rev. Lett. **129**, 113601 (2022).
[46] C. Leefmans, A. Dutt, J. Williams, L. Yuan, M. Parto, F. Nori, S. Fan, and A. Marandi, Topological dissipation in a time-multiplexed photonic resonator network, Nat. Phys. **18**, 442 (2022).
[47] S. Weidemann, M. Kremer, S. Longhi, and A. Szameit, Topological triple phase transition in non-Hermitian Floquet quasicrystals, Nature (London) **601**, 354 (2022).
[48] C. Yuce and H. Ramezani, Non-Hermitian edge burst without skin localization, Phys. Rev. B **107**, L140302 (2023).
[49] H. Jiang and C. H. Lee, Dimensional transmutation from non-Hermiticity, Phys. Rev. Lett. **131**, 076401 (2023).
[50] A. Schreiber, K. N. Cassemiro, and V. Potoček, A. Gábris, P. J. Mosley, E. Andersson, I. Jex, and C. Silberhorn, Photons walking the line: A quantum walk with adjustable coin operations, Phys. Rev. Lett. **104**, 050502 (2010).
[51] A. Schreiber, A. Gábris, P. P. Rohde, K. Laiho, M. Štefaňák, V. Potoček, C. Hamilton, I. Jex, and C. Silberhorn, A 2D quantum walk simulation of two-particle dynamics, Science **336**, 55 (2012).
[52] M. Wimmer, H. M. Price, I. Carusotto, and U. Peschel, Experimental measurement of the Berry curvature from anomalous transport, Nat. Phys. **13**, 545 (2017).
[53] H. Chalabi, S. Barik, S. Mittal, T. E. Murphy, M. Hafezi, and E. Waks, Synthetic gauge field for two-dimensional time-multiplexed quantum random walks, Phys. Rev. Lett. **123**, 150503 (2019).
[54] See Supplemental Material at http://link.aps.org/supplemental/10.1103/PhysRevLett.132.203801 for details of topological properties, imaginary gap closing, and non-Hermitian skin effect of the theoretical model, and our experimental implementation of Floquet operator, which includes Refs. [8,15–17,21].
[55] D. Leykam and D. Smirnova, Probing bulk topological invariants using leaky photonic lattices, Nat. Phys. **17**, 632 (2021).
[56] L. Xiao, W. Xue, F. Song, Y. Hu, W. Yi, Z. Wang, and P. Xue, Observation of non-Hermitian edge burst in quantum dynamics, arXiv:2303.12831.